SLAC PUB-4790
November 1988
(N)

22. Positron Emission Tomography Applications of EGS*

A. Del Guerra† and Walter R. Nelson‡

Department of Physics, University of Pisa
Piazza Torricelli 2, I-56100, Pisa, Italy†

Stanford Linear Accelerator Center, Stanford University
Stanford, CA 94309‡

22.1 PRINCIPLES OF POSITRON EMISSION TOMOGRAPHY

The use of positron emitters in medical imaging was first suggested by Wrenn and coworkers[1], and Sweet[2], and the first prototype Positron Emission Tomography (PET) scanner was built by Brownell and Sweet[3] as shown in Fig. 22.1. A radiopharmaceutical labeled with a positron emitter is distributed within a biological target. The emitted β^+ annihilates with an electron of the surrounding tissue to produce two photons of 511 keV back-to-back (in the CM system). By detecting these two gammas in coincidence, one constrains the annihilation event to the volume spanned by the two detectors. The original distribution of radioisotope is reconstructed from a series of "projections", obtained by moving and rotating the scanner around the patient. The "electronic collimation" avoids the use of passive collimators (typical transmission efficiency $10^{-4} - 10^{-3}$) which are necessary in Single Photon Emission Computed Tomography (SPECT) with γ-emitting radionuclides; this implies not only a reduction of the radiation dose delivered to the patient, but also a higher spatial resolution and a better quantization of the imaging results.

22.2 PHYSICAL PROCESSES IN PET

Many physical processes are involved in the detection in coincidence of the two annihilation quanta.

22.2.1 Positron Emitters

The commonly used positron emitters are listed in Table 22.1, together with the lifetime and the mean energy of the β spectrum[4]. Because carbon, nitrogen and oxygen are the most important constituent elements of the human body, the so-called physiological β^+ isotopes (^{11}C, ^{13}N, ^{15}O) are particularly attractive for the monitoring of any

* Work supported in part by the Department of Energy, contract DE-AC03-76SF00515.

† Present address: Department of Physics
University of Napoli
Napoli, Italy

‡ Permanent address

Chapter 22 (Pages 469-484) in "Monte Carlo Transport of Electrons and Photons," T.M. Jenkins, W.R. Nelson, and A. Rindi, Editors (Plenum Publishing Co. 1988)

metabolic pathway. However, due to their very short lifetime, a dedicated cyclotron ("in loco") is required for their production. ^{18}F is also commonly used, especially to label deoxiglucose (FDG). ^{68}Ga and ^{82}Rb, although non-"physiological" isotopes, are readily available from commercial generators, and their use is increasing rapidly.

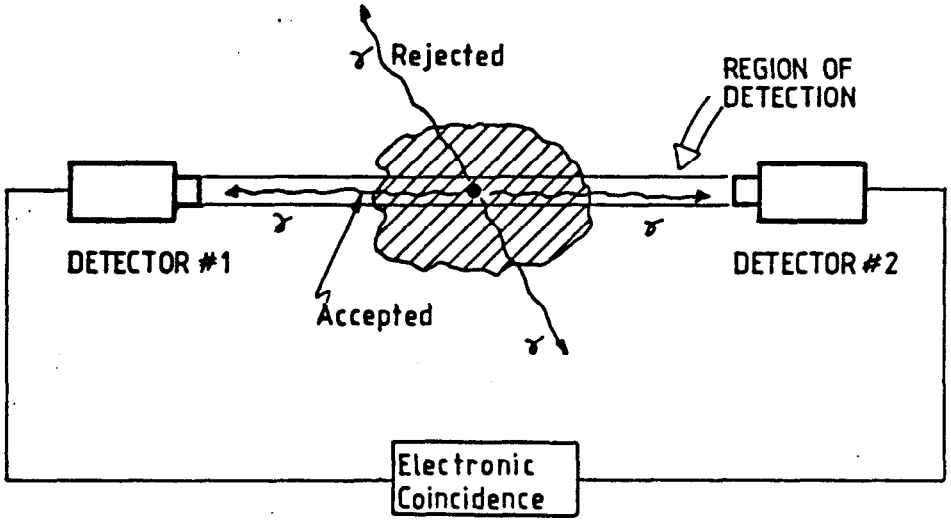

Figure 22.1. Schematic drawing of the first PET scanner[5].

Table 22.1. Positron Emitters Most Used in PET.

Radioisotope	$\tau_{\frac{1}{2}}$ (minutes)	Mean energy of β^+ spectrum T_{mean} (MeV)
^{11}C	20.4	0.385
^{13}N	10.0	0.491
^{15}O	2.0	0.735
^{18}F	109.8	0.242
$(^{82}Sr) \Rightarrow {}^{82}Rb$	1.3	1.410
$(^{68}Ge) \Rightarrow {}^{68}Ga$	68.1	0.740

22.2.2 Positron Range

The β^+ is emitted with a continuous energy spectrum. Before annihilating "at rest" (the *in-flight* annihilation probability is at most a few percent), the positron travels a finite range, which depends upon its energy (see Table 22.1). The range in tissue varies from a fraction of a mm for ^{18}F (which has the lowest energy) to several mm for ^{82}Rb (*e.g.*, see Derenzo[6]).

22.2.3 Positron Annihilation

The annihilation of the positron at rest with an electron at rest would imply the emission of two γ's in opposite directions. However, due to the Fermi motion, the distribution is almost Gaussian around 180^0. In water (tissue), the FWHM is ~ 0.5 degrees[7].

22.2.4 Scatter in Tissue

The mean free path of a 511-keV photon in water is $\sim$ 10 cm. The human head or chest are roughly two mean free paths thick. This results in a heavy loss of coincident photons; only 20–30% of the two γ's will reach the detector unaffected. Furthermore, a fraction of the scattered photons will still produce coincidence events, contributing a distributed background which gives rise to "projections" from "non-existing source" positions, thus smearing the resolution and decreasing the contrast of the object.

22.2.5 Interaction Within the Detector

The detection of the two photons depends upon the attenuation coefficient and the stopping power of the detector, and its "quantum efficiency", *i.e.*, the efficiency in converting the energy loss into useful digital information. The type of detector chosen, (scintillator crystal, gaseous detector, *etc.*) is a major part of the design of a PET camera, as will be discussed in the next section.

22.3 THE PET CAMERA

The design of PET cameras varies greatly. From the original two detector scanner moving and rotating around the patient (*e.g.*, Fig. 22.1), more complex solutions have been implemented, such as two opposite and rotating Anger cameras, a planar annular ring of scintillators, large-area planar geometries, and multi-ring configurations (see Fig. 22.2).

For the design of a PET camera, the following requirements are important:

- a high detection efficiency for 511-keV γ-rays,
- a short temporal resolution for the coincidence,
- a high spatial resolution,
- a large solid angle coverage.

Of course, not all the parameters can be optimized at the same time. A solution which best fulfills one requirement may be rather loose on another; hence, different designs cannot be compared against one or two parameters, but only in terms of their global performance—*i.e.*, the quality of the image obtained in a given time with a certain amount of activity concentration in tissue.

22.3.1 Scintillator Multicrystal Detector

The first generation PET camera was made as a single ring of NaI(Tℓ) scintillator crystals(*e.g.*, Fig. 22.2b). In order to increase the sensitivity, other scintillators are now used (see Table 22.2). Bismuth Germanate ($Bi_4Ge_3O_{12}$, simply called BGO) is the highest

density, highest Z scintillator material available. Although the photopeak-to-Compton ratio is not as good as for NaI, (thus producing a slightly worse energy resolution at 511 keV), BGO is the best scintillator for totally absorbing 511-keV photons in small crystals; this makes it possible to reduce the crystal size, and thus increase the spatial resolution without adding cross-talk and multiple-hit problems. Furthermore, to increase the axial solid-angle coverage, multi-ring solutions (*e.g.*, Fig. 22.2d) usually are adopted.

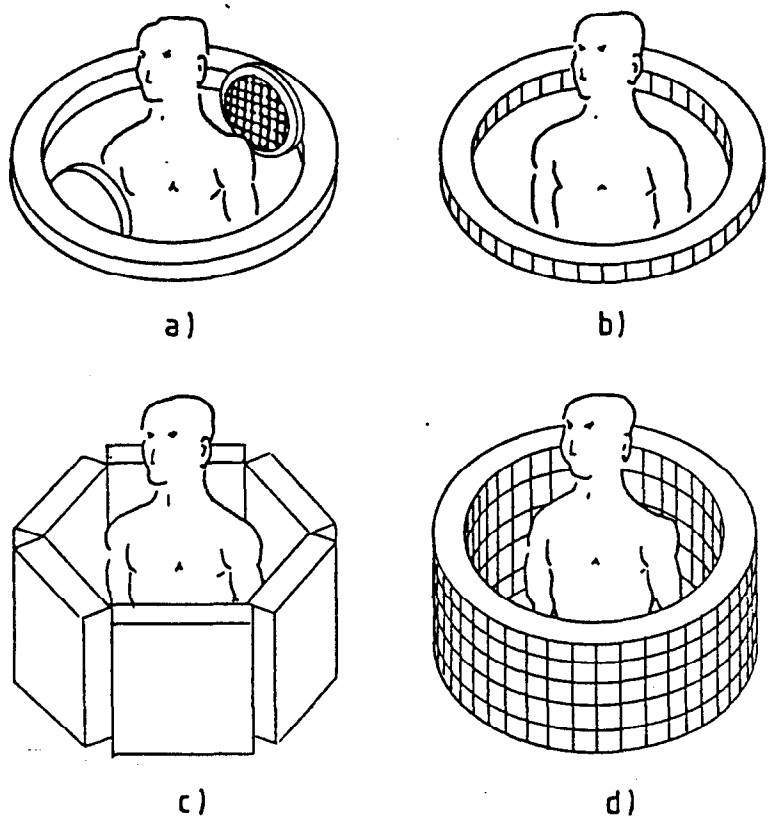

Figure 22.2. Examples of PET camera configurations: a) two opposite Anger cameras; b) single ring; c) large-area hexagon planar camera; d) multi-ring[5].

An alternative solution is the use of faster scintillators to decrease the time coincidence window, and thus to reduce the accidental contamination so as to have a better signal-to-noise ratio. Additionally, by measuring the difference in time between the arrivals of the two photons, one could identify directly the source position (or at least reduce the position uncertainty) along the line-of-flight. This technique is called Time Of Flight PET (TOFPET). With scintillators such as CsF and BaF_2 which give a time resolution of 400 ps, it is possible to determine the source position to within $\sim$ 6 cm along the photon's flight path.

Table 22.2. Main Properties of Various Scintillators Used in PET Cameras.

Crystal	NaI(Tℓ)	BGO	CsF	BaF_2
Density (g/cm^3)	3.67	7.13	4.64	4.89
Atomic Number	11, 53	83, 32, 8	55, 9	56, 9
Linear Attenuation Coefficient at 511 keV (cm^{-1})	0.34	0.92	0.44	0.47
Scintillation Decay Time (ns)	250	300	5	0.8/620
Emission Wavelength (nm)	410	480	390	225/310
Energy Resolution at 511 keV (FWHM)	> 7%	> 10%	23%	13%
Index of refraction	1.85	2.15	1.48	1.59
Hygroscopic	Yes	No	Very	No

A spatial resolution of 3-4 mm is considered to be the practical limit for PET imaging, if one takes into account the contributions due to the non-collinearity of the two photons, the positron range, and the limited statistics. Thus, it is not worthwhile building detectors with an intrinsic resolution much below that value. To improve the spatial resolution in a discrete system such as in a many-scintillator PET camera, one can simply use smaller crystals, for instance 4 mm instead of the standard 8-10 mm size. This, of course, implies the use of appropriate phototubes and electronics, increasing the cost and the complexity of the tomograph.

22.3.2 Gas Detector

Another interesting approach is the use of large-area, position-sensitive gaseous detectors, such as the MultiWire Proportional Chamber (MWPC). This type of detector[8] was originally designed for high-energy physics experiments. It basically consists of a gas-filled chamber with three wire planes, the central one kept at positive voltage. If an ionization is produced in the gas region, the electrons are drifted towards the anode plane and produce an avalanche (around an anode wire) which can be detected directly from the anode signal or from the signals induced on the cathode planes.

The use of MWPC's for PET is particularly attractive because of their very good spatial resolution: some hundreds of μm are easily achieved along the anode wire direction, whereas in the other direction, the spatial resolution is determined by the anode wire pitch (typically 2 mm). Furthermore, large areas are easy to cover. However, an obvious limitation in the use of MWPC's for γ-imaging arises from the difficulty of stopping the photon in the gas. For instance, the photopeak efficiency at 511 keV in 1 cm of Xe at 10 atmospheres is still much below 1%. It is then necessary to use high-Z, high-density converters.

22.4 USE OF MONTE CARLO CODES IN TOMOGRAPH DESIGN

The construction of a tomograph calls for a careful planning of the detector type, the detectors arrangements, the diameter of the gantry, *etc.* Although experimental work on a smaller prototype is mandatory, a complete simulation of the tomograph by Monte Carlo technique is very useful to evaluate the performance and optimize the design.

Monte Carlo radiation transport codes have been succesfully used by various authors to cover individual aspects of a PET design.

Derenzo[6] has studied the annihilation point-spread function of various positron emitters in water in order to deconvolve the range contribution from the reconstructed image and obtain a better spatial resolution. The same physical process has been investigated by Iida *et al*[9], who studied the reduction of the annihilation point-spread function by applying a magnetic field, expecially for high-energy emitters such as ^{82}Rb. Derenzo[10]and Derenzo and Riles[11] have studied the efficiency of various scintillator-photomultiplier systems to tailor the dimension of the crystal and the thickness of the absorption septum between two crystals, to minimize cross-talk, and to maximize the spatial resolution.

The idea of using Monte Carlo codes to optimize the geometry of a single-slice tomograph for a given field of view has been pursued by Lupton and Keller[12]. They have evaluated the accidental/true coincidence ratio and the scattered-coincidences profile for an annular ring geometry and various object/gantry diameter ratios. In this case, a Monte Carlo code could give unique information because it can "tag" the scattered and unscattered events, which are indistinguishable in the experimental situation.

In all of these examples and in many others, Monte Carlo codes are used to simulate specific sections, or selected performances of a tomograph. In the next section, we will present an example of a very ambitious program we have been carrying out to simulate completely a large-area 3-D tomograph by means of the EGS4 code[13].

22.5 AN APPLICATION: USE OF EGS4 FOR THE HISPET DESIGN

A fully 3-D large-area positron camera (HIgh Spatial resolution Positron Emission Tomograph) has been proposed[14] which consists of six modules arranged so as to form the lateral surface of a hexagonal prism (see Fig. 22.3). The type of detector chosen is a gaseous detector with an appropriate high-density converter. We have developed, as a converter, a matrix of resistive lead-glass tubing[15] (also see Section 28.2.4).

An electric field is applied along the converter so that the photoelectrons (produced by the γ interaction within the converter walls) are drifted out of the converter to the avalanche region of the MWPC. A schematic drawing of a MWPC equipped with a lead-glass tube converter is shown in Fig. 22.4.

Each module of HISPET will have two MWPC's, each with two 1-cm thick converter planes of lead-glass tubing (0.5 mm and 0.6 mm, inner and outer diameter, respectively). In order to study the efficiency of this type of converter and to evaluate the performance of the tomograph, two different EGS4 User Codes (UCCELL and UCPET) were used, as described in the following sections.

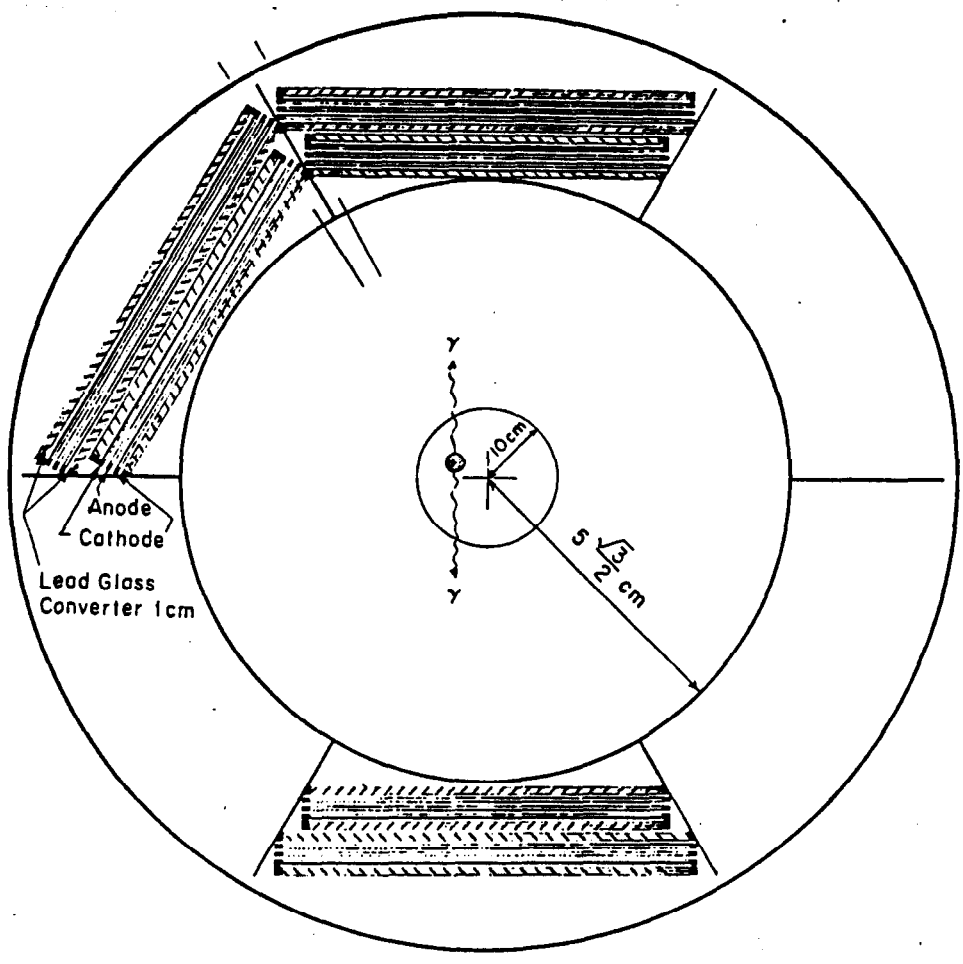

Figure 22.3. The HISPET project. For simplicity only three modules are shown[14].

22.5.1 The Converter Efficiency Code (UCCELL)

The converter is made of glass capillaries of high lead content, fused to form honeycomb matrices. In order to calculate the efficiency versus photon energy, an EGS4 User Code (UCCELL) with a relatively simple geometry, based on the *unit cell* concept, was created[16]—*i.e., two concentric cylinders inside a box* (see Fig. 22.5).

Photons randomly irradiate the top face of the cell at 90^0 ($\pm 3.5^0$), the same geometry as used in the experimental measurement[17] . All particles are transported inside the cell until they reach energy cutoffs (10 keV and 1 keV for e^- and γ, respectively), exit the top or bottom, or exit the sides. In the latter case, in order to characterize fully the converter with a multitude of contiguous holes, the particles are re-transported into the unit cell by making the appropriate coordinate translation while maintaining the direction of motion. If the electron produced by the photon interaction enters the inner region of the cell, it is considered to be *detected*, irrespective of its energy at that point.

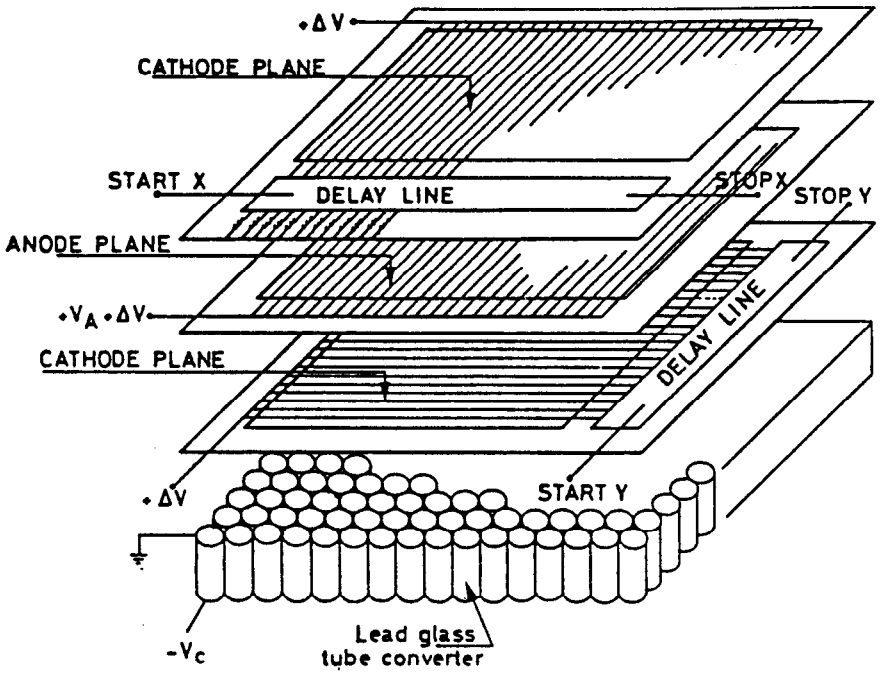

Figure 22.4. Schematic drawing of a MWPC equipped with a lead-glass tube converter plane for PET imaging[14].

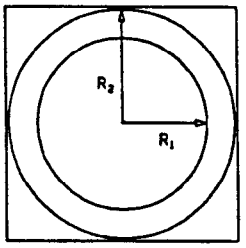

Figure 22.5. The *unit cell* geometry used in UCCELL.

The probability that an electron will reach a hole depends on its energy, where it is created, and its direction of motion. In UCCELL, the energy released by photon interactions was scored into two separate histograms—detected events (*i.e.*, when an electron enters a hole), and total events. The ratio of the distributions provided a measure of the detection probability (averaged over position and direction) as a function of the electron kinetic energy. The probability table thus created by UCCELL was then

used in the second EGS4 User Code (UCPET) for the study of the general performance of HISPET (see next section)* .

Various combinations of inner and outer diameters were chosen with the length of the cell fixed at 1 cm. Various types of lead glass with different percentages of PbO and different densities were also simulated. Figure 22.6 shows the calculated efficiency of the converter as a function of the photon energy for three ID/OD tube converters, compared with our experimental data[17] obtained with 80% PbO lead glass (density 6.2 g/cm^3). Figure 22.7 shows the calculated efficiency for 511-keV photons versus the diameter of the tube at a fixed OD/ID ratio of 1.2 for the various lead glass types. Figure 22.8 shows the calculated efficiency versus wall thickness for a given inner diameter of the tube for various percentages of lead content. These results have made it possible to optimize the lattice of the converter.

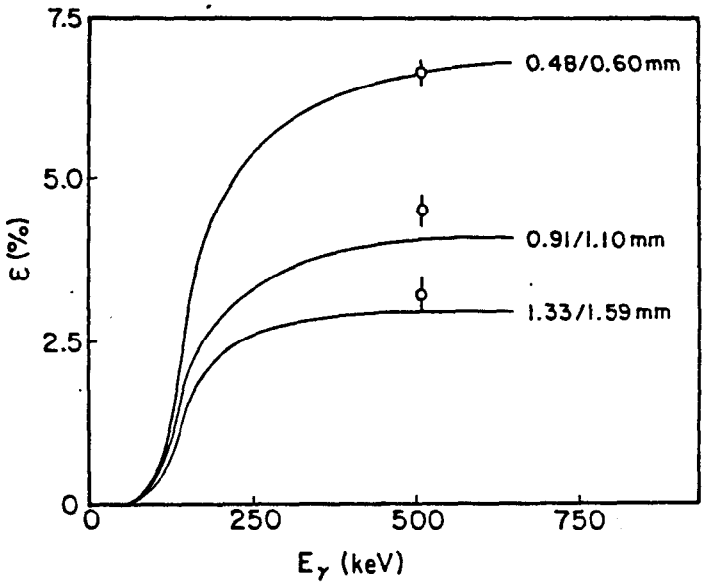

Figure 22.6. Calculated efficiency of a 1-cm thick converter as a function of the photon energy for different combinations of inner and outer diameters (solid lines); o-experimental data[18].

22.5.2 Evaluation of the HISPET Performance (UCPET)

A full three-dimensional simulation of the HISPET was performed using the EGS4 User Code, UCPET[19] , according to the following scheme:

1. Generation of the positron coordinates, direction, and energy. The latter was sampled according to the energy spectrum of the selected radioisotope; theoretical beta spectra[20] (corrected for screening) were introduced into EGS4 in the form of look-up tables. The following isotopes were considered: ^{11}C, ^{13}N, ^{15}O, ^{18}F, ^{19}Ne, ^{38}K, ^{68}Ga, and ^{82}Rb.

* Note: Limiting the energy loss along a charged particle track by means of ESTEPE (*e.g.*, see Chapter 5) had not been introduced at the time of these calculations (1982).

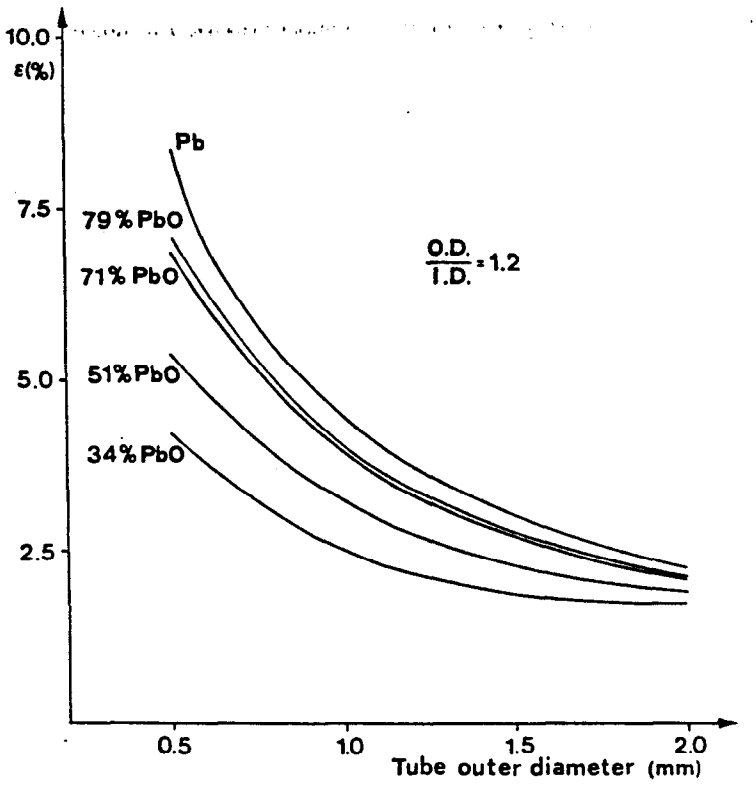

Figure 22.7. Calculated efficiency of a 1-cm thick converter as a function of the tube outer diameter for an outer/inner diameter ratio of 1.2. Note: Various PbO proportions correspond to commercial glasses used experimentally; efficiency curve for pure lead drawn for comparison[18].

2. Transport and annihilation of the positron in the phantom. In principle, due to the structure of EGS4 itself, it is possible to simulate any type of phantom, although only cylindrical and spherical geometries were implemented in the simulation. The positron was followed in the phantom until it reached the lower energy cutoff of 10 keV, when it was forced to annihilate as if at rest. In addition to Bhabha scattering and continuous energy loss, EGS4 also considers annihilation in flight as a discrete Monte Carlo process. Once the annihilation takes place, the angular distribution is properly taken into account for two photons, both for annihilation at rest and in flight, the latter probability being at most a few per cent for the highest energy radioisotope. Figure 22.9 shows the differential probability of annihilation per unit distance from the source in water for various radioisotopes.

3. Transport of annihilation quanta from within the phantom to the detector. During this step of the program, all charged particles that are generated are immediately discarded. If the photon emerges from the phantom with an energy greater than the cutoff energy (1 keV), it is further transported to the detector.

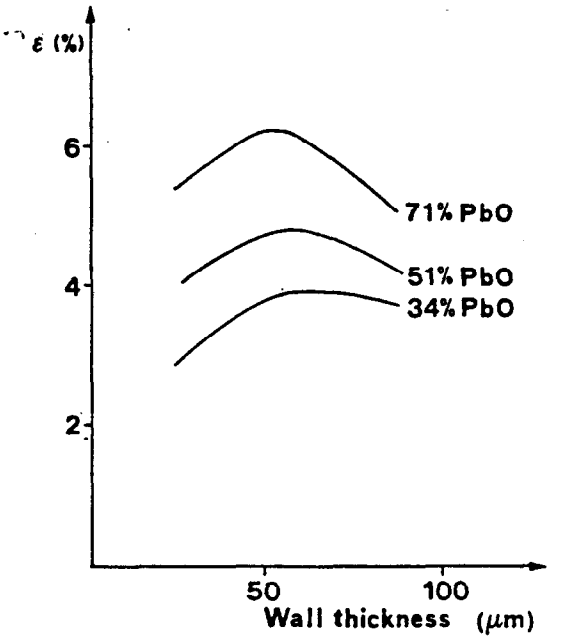

Figure 22.8. Efficiency of 1-cm thick converter of 0.5-mm inner diameter versus the wall thickness for various Pb compositions[18].

4. Simulation of the three-dimensional geometry of the detector. The implementation of any particular geometry is left up to the discretion of the user of EGS4. Accordingly, the hexagonal prism geometry of HISPET was simulated by means of the geometry macro package that is distributed with the EGS4 Code System. The geometry was fairly precise, and included the four planes of converters and the two MWPC sensitive regions for each module.

5. Interaction of the photon within the detector. To simulate the interaction of the photon within the detector, the actual lead-glass honeycomb geometry was approximated by a solid converter, the density of which was reduced by the packing fraction (*i.e.*, the ratio of the covered to total area).

6. Scoring of the events. Those events where only one or both photons detected are accounted for, and the single and coincidence rates are tabulated. Finally, to study the spatial resolution of HISPET, simple histograms are produced using coincidence events both in opposite and non-opposing modules.

The SLAC Unified Graphics System[21] was also used in UCPET in order to provide a means of visualizing the various interaction sequences that lead to both good and bad *event scenarios*. An example is presented in Fig. 22.10 showing two orthogonal views of the tomograph and two photon tracks (*i.e.*, solid and dotted lines).

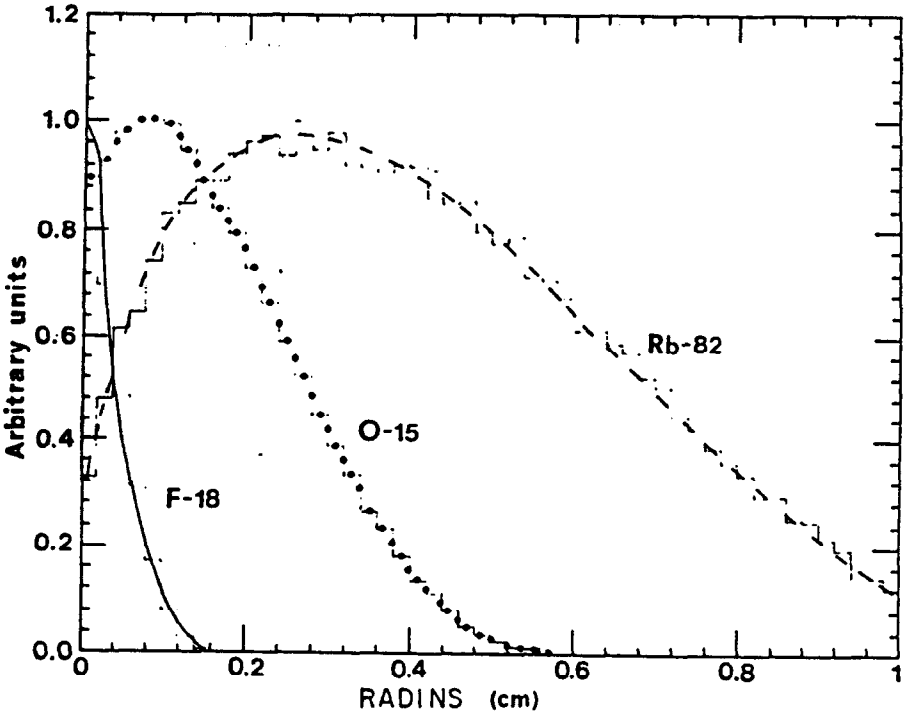

Figure 22.9. Differential probability of annihilation per unit distance from the source in water for several β^+ radioisotopes (each curve is normalized to a maximum value of 1.0 for purposes of comparison[19]).

Information related to the event history for each photon is printed in the two corresponding boxes, according to the following key:

S — Indicates the *sector* where the interaction took place (1-6). The value of 0 is assumed if the interaction is in the phantom itself.

D — Indicates which *converter* ("detector") is involved (first, second, third or fourth).

T — Identifies the *type* of interaction (C for Compton, P for photoelectric).

GE1 — Photon energy *before* the interaction.

GE2 — Photon energy *after* the interaction.

EKE — Electron *kinetic energy*.

TD — *Distance* of the interaction point from the end of the tube, which is proportional to the drift time to the MWPC.

In the example presented in Fig. 22.10, the first photon (solid line and solid box) interacts twice in sector 1, both times in converter 3. The first results in a Compton electron of 277 keV at a distance of 0.501 cm from the end of the tube; the second in a photoelectron of 146 keV at a distance of 0.581 cm from the end of the tube. The Compton or photoelectron is assumed to be detected with a probability as given by the appropriate probability table calculated from the *unit cell* simulation (*i.e.*, UCCELL).

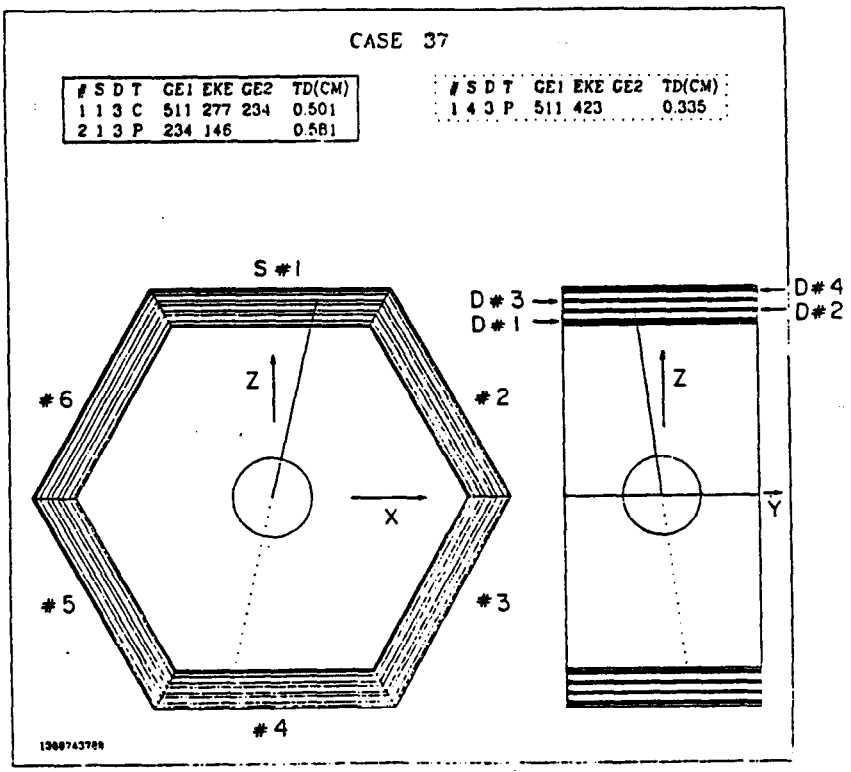

Figure 22.10. Typical display of a "good" 2-γ event[19](see text for an explanation).

The second photon (dotted line and dotted box) makes only one interaction, resulting in a 423-keV photoelectric electron in the third converter of sector 4 (0.335 cm from the end of the tube).

If one photon produces more than one detected electron in the same module, only the earliest electron (that nearest to the anode plane of the MWPC) is retained. The real coordinate along the thickness of the converter is substituted by half the thickness so as to account for the parallax error. The x and y finite resolution of the MWPC are also simulated directly within EGS4/UCPET by sampling from appropriate Gaussian distributions, and the final position is checked against spatial cutoffs.

22.5.3 Image Reconstruction From EGS4-Simulated Data Output

Output from EGS4 (*i.e.*, "events") are stored onto permanent memory for subsequent analysis, as if it were *real*. In particular, the coincidence data are analyzed by the 3-D filtered back-projection algorithm[22], which in fact has been tested and optimized on the simulated data, and is now used on the first real data from a HISPET prototype[23].

Figure 22.11 shows the spatial resolution which is obtained taking a profile through the central plane of the reconstructed image for a point-like ^{18}F source embedded in a head water phantom at the center of the tomograph.

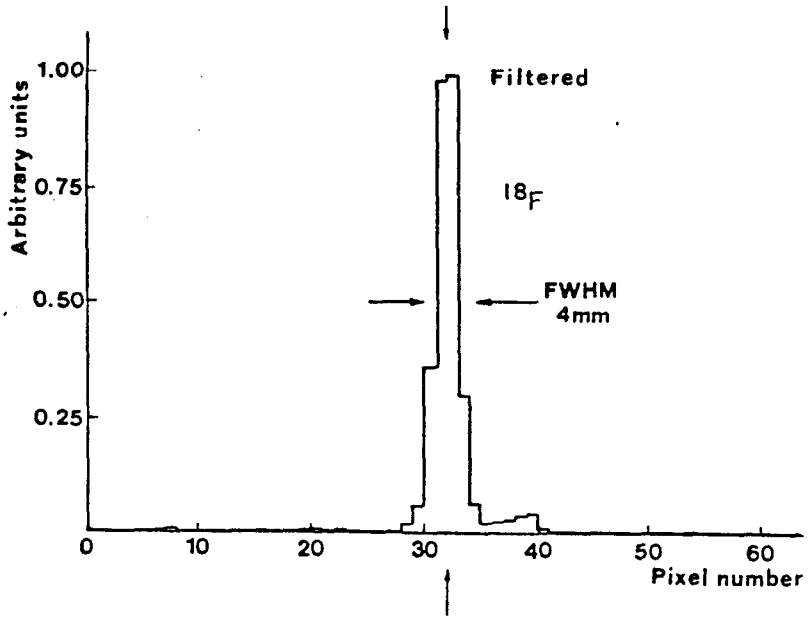

Figure 22.11. Spatial resolution of a ^{18}F point-like source embedded in a 10 cm radius water phantom (sphere), at the center of the HISPET tomograph. Data were simulated by Monte Carlo and reconstructed by the filtered back-projection 3-D algorithm[19].

It is also possible to produce a sample of the accidental coincidences by randomly regrouping two-by-two the interactions points. Again, the scattered events in the phantom keep their signature in the simulation, and their effects on the spatial resolution can be singled out and quantified.

22.6 SUMMARY

The simulation of HISPET by means of the EGS4 Code System has proved to be very useful, especially as an aid in selecting the design parameters of the project. In particular, the user has the capability of using software to turn on and off various processes and quantities of interest. This feature of EGS4 has been used to:

—independently study the geometric and total efficiency of the modules and of the entire tomograph;

—investigate the different contributions to the spatial resolution—*i.e.*, due to source localization, positron range, two-gamma non-collinearity, parallax error, intrinsic detector resolution, Compton scattering in the phantom, *etc.*

Because the simulation is purely analog in nature, it is inherently inefficient. About 200 positrons/second can be generated, and the subsequent progeny tracked, on an IBM-3081 mainframe computer. One can, however, take advantage of the modularity of EGS4/UCPET in order to produce a large sample of data, and then to apply the various software cuts, which simulate the configuration being studied.

REFERENCES

1. E. R. Wrenn, M. L. Good and P. Handler, "The Use of Positron Emitting Radioisotopes for the Localization of Brain Tumours", Sci. 113 (1951) 525.
2. W. H. Sweet, "Uses of Nuclear Disintegration in the Diagnosis and Treatment of Brain Tumours", New Engl. J. Med. 245 (1951) 875.
3. G. L. Brownell and W. H. Sweet, "Localization of Brain Tumours With Positron Emitters", Nucleonics 11 (1953) 40.
4. E. Browne and R. B. Firestone, *Table of Radioactive Isotopes*, edited by V. S. Shirley, (John Wiley & Sons, New York, 1986).
5. A. Del Guerra, "Positron Emission Tomography", Physica Scripta T19 (1987) 481.
6. S. E. Derenzo, "Precision Measurements of Annihilation Point Spread Function for Medically Important Positron Emitters", in *Positron Annihilation*, edited by R. R. Hasiguti and K. Fujiwara, (Japan Institute of Metals, Sendai, Japan, 1979); 819.
7. P. Colombino, B. Fiscella and L. Trossi, "Study of Positronium in Water and Ice from 22 to -144 °C by Annihilation Quanta Measurements", Nuovo Cimento 38 (1965) 707.
8. F. Sauli, "Principles of Operation of MultiWire Proportional and Drift Chambers", CERN report 77-06 (1977).
9. H. Iida, I. Kanno, S. Miura, M. Murakami, K. Takahashi and K. Uemura, "A Simulation Study of a Method to Reduce Positron Annihilation Spread Distributions Using a Strong Magnetic Field in PET", IEEE Trans. Nucl. Sci. NS-33 (1986) 597.
10. S. E. Derenzo, "Monte Carlo Calculations of the Detection Efficiency of Arrays of NaI(Tℓ), BGO, CsF, Ge, and Plastic Detectors for 511 keV Photons", IEEE Trans. Nucl. Sci. NS-28 (1981) 131.
11. S. E. Derenzo and J. Riles, "Monte Carlo Calculations of the Optical Coupling Between Bismuth Germanate Crystals and Photomultiplier Tubes", IEEE Trans. Nucl. Sci. NS-29 (1982) 191.
12. L. R. Lupton and N. A. Keller, "Performance Study of Single-Slice Positron Emission Tomography Scanners by Monte Carlo Techniques", IEEE Trans. Med. Imag. MI-2 (1983) 154.
13. W. R. Nelson, H. Hirayama and D. W. O. Rogers, "The EGS4 Code System", Stanford Linear Accelerator Center report SLAC-265 (1985).
14. A. Del Guerra, G. K. Lum, V. Perez-Mendez and G. Schwartz, "The HISPET Project: State of the Art", in *Positron Annihilation*, edited by P. C. Jain, R. M. Singru and K. P. Gopinathan, (World Scientific Publishing Co., Singapore, 1985); 810.
15. M. Conti, A. Del Guerra, R. Habel, T. Mulera, V. Perez-Mendez and G. Schwartz, "Use of a High Lead Glass Tubing Projection Chamber in Positron Emission Tomography and in High Energy Physics", Nucl. Instr. Meth. A255 (1987) 207.
16. A. Del Guerra, V. Perez-Mendez, G. Schwartz, and W. R. Nelson, "Design Considerations for a High Spatial Resolution Positron Camera with Dense Drift Space MWPCs", IEEE Trans. Nucl. Sci. NS-30 (1983) 646.

17. R. Bellazzini, A. Del Guerra, M. M. Massai, W. R. Nelson, V. Perez-Mendez and G. Schwartz, "Some Aspects of the Construction of HISPET: HIgh Spatial Resolution Positron Emission Tomograph", IEEE Trans. Nucl. Sci. NS-31 (1984) 645.

18. A. Del Guerra, A. Bandettini, M. Conti, G. De Pascalis, P. Maiano, C. Rizzo, and V. Perez-Mendez, "3-D PET with MWPCs: Preliminary Tests with the HISPET Prototype", Nucl. Instr. Meth. A269 (1988) 425.

19. A. Del Guerra, M. Conti, W. R .Nelson, R .Porinelli, and C. Rizzo, "3-D Imaging with a 3-D PET: A Complete Simulation of the HISPET Tomograph", in *Intern. Workshop on Physics and Engin. of Computerized Multidimensional Imaging and Processing*, edited by O. Nalcioglu, Z. H. Cho, and T. F. Budinger, (SPIE 671, 1986) 34.

20. E. J. Konopinski and M. E. Rose, "The Theory of Nuclear Beta-Decay", in *Alpha-, Beta-, Gamma-Ray Spectroscopy*, K. Siegbahn (Ed.) (North-Holland Publishing Co., 1965); p. 1327; U. Fano, "Tables for the Analysis of the Beta Spectra", National Bureau of Standards, Applied Mathematics Series, Volume 13 (1952).

21. R. C. Beach, "The Unified Graphics System for FORTRAN 77: Programming Manual", SLAC Computation Research Group technical memorandum CGTM 203 (November 1985 revision).

22. C. Rizzo, M. Conti and A. Del Guerra, "Evaluation of the Imaging Capabilities of HISPET", Physica Medica 1 (1987) 19.

23. A. Del Guerra, A. Bandettini, M. Bucciolini, M. Conti, G. De Pascalis, P. Maiano, V. Perez-Mendez and C. Rizzo, "First Experimental Results from a High Spatial Resolution PET Prototype", Proc. Ninth Annual Conf. IEEE Engin. in Med. and Biol. Society, Boston, MA (November 13-16, 1987); 1010.